Electronic Supplementary Material

In situ separator modification via CVD-derived N-doped carbon for highly reversible Zn metal anodes

Xianzhong Yang[1], Weiping Li[1], Jiaze Lv[1], Guojie Sun[1], Zixiong Shi[1], Yiwen Su[1], Xueyu Lian[1,2], Yanyan Shao[1], Aomiao Zhi[3], Xuezeng Tian[3], Xuedong Bai[3], Zhongfan Liu[1,2,4] (✉), and Jingyu Sun[1,2] (✉)

[1] *College of Energy, Soochow Institute for Energy and Materials Innovations (SIEMIS), Jiangsu Provincial Key Laboratory for Advanced Carbon Materials and Wearable Energy Technologies, Soochow University, Suzhou 215006, China*
[2] *Beijing Graphene Institute (BGI), Beijing 100095, China*
[3] *Institute of Physics, Chinese Academy of Sciences, Beijing 100190, China*
[4] *Center for Nanochemistry (CNC), College of Chemistry and Molecular Engineering, Peking University, Beijing 100871, China*

Supporting information to https://doi.org/10.1007/s12274-021-3957-z

Supporting Figure

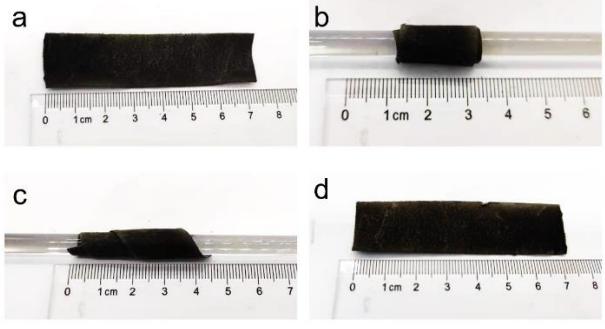

Figure S1 (a) Digital photo of NC/GF prior to rolling and twisting. (b,c) Digital photos of the rolling and twisting states of NC/GF. (d) Digital photo of NC/GF after rolling and twisting.

Figure S2 Optical images of NC/GF separator before and after air plasma treatment. (a) NC/GF separator before air plasma treatment. (b) The front side of NC/GF separator after air plasma treatment. (c) The rear side of NC/GF separator after air plasma treatment. The color of the rear side changes from black to white, confirming the NC species was removed thoroughly on this side.

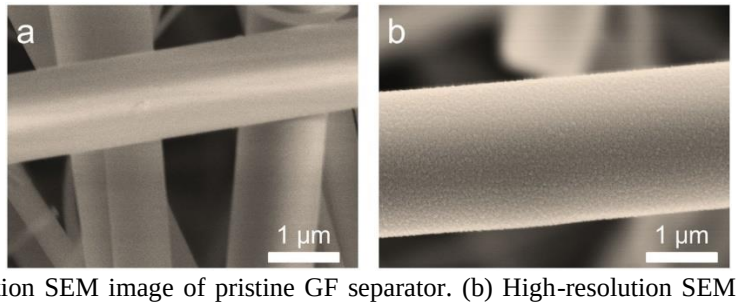

Figure S3 (a) High-resolution SEM image of pristine GF separator. (b) High-resolution SEM image of prepared NC/GF separator.

Address correspondence to Zhongfan Liu, zfliu@pku.edu.cn; Jingyu Sun, sunjy86@suda.edu.cn

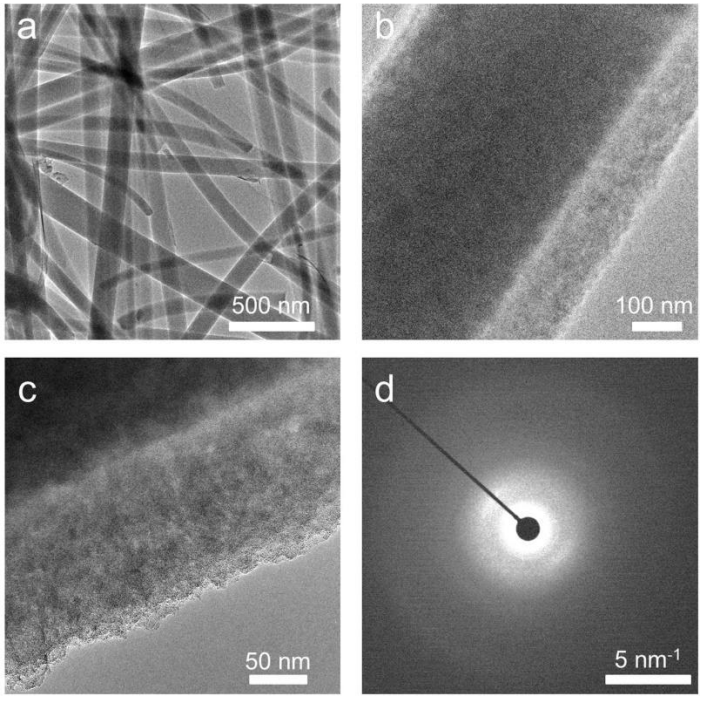

Figure S4 (a-c) TEM images of the as-fabricated NC/GF separator. (d) The corresponding SAED pattern.

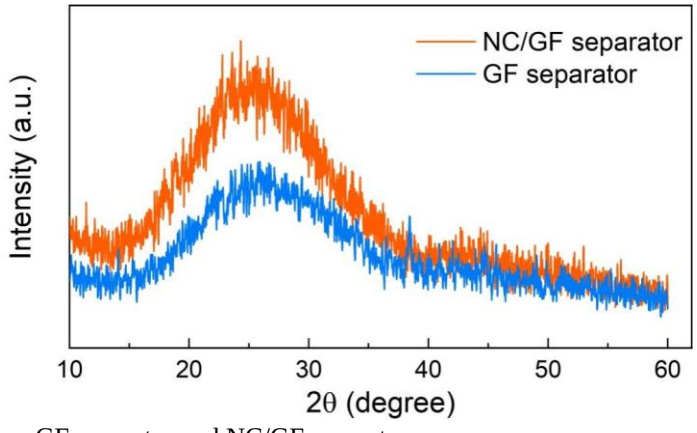

Figure S5 XRD patterns of bare GF separator and NC/GF separator.

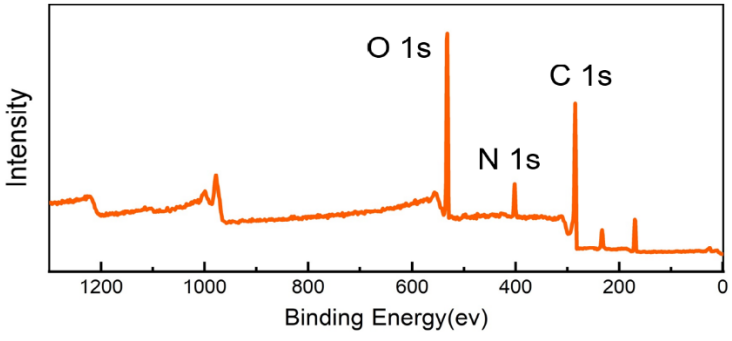

Figure S6 XPS survey spectrum of NC/GF separator.

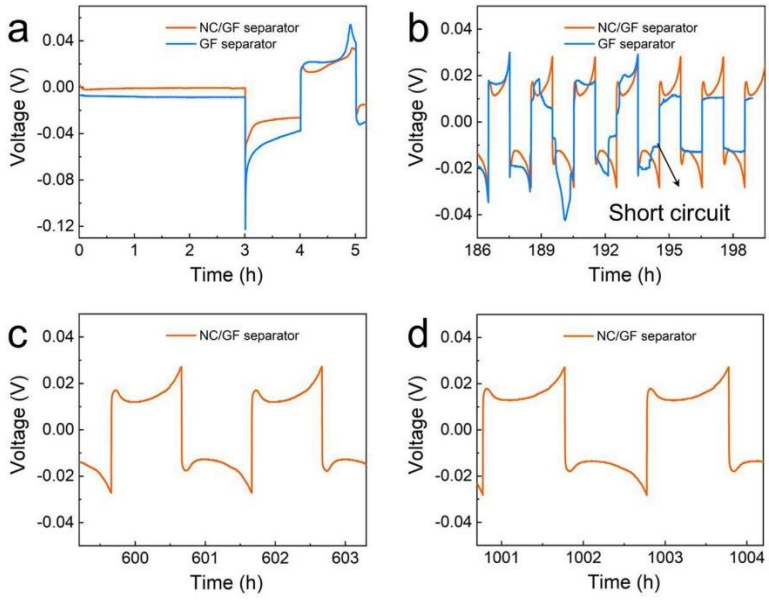

Figure S7 Enlarged voltage profiles at selected cycles in Fig. 2d. (a) The initial rest state and the 1st cycle. (b) The 91st-98th cycles. (c) The 298th-299th cycles. (d) The 499th-500th cycles.

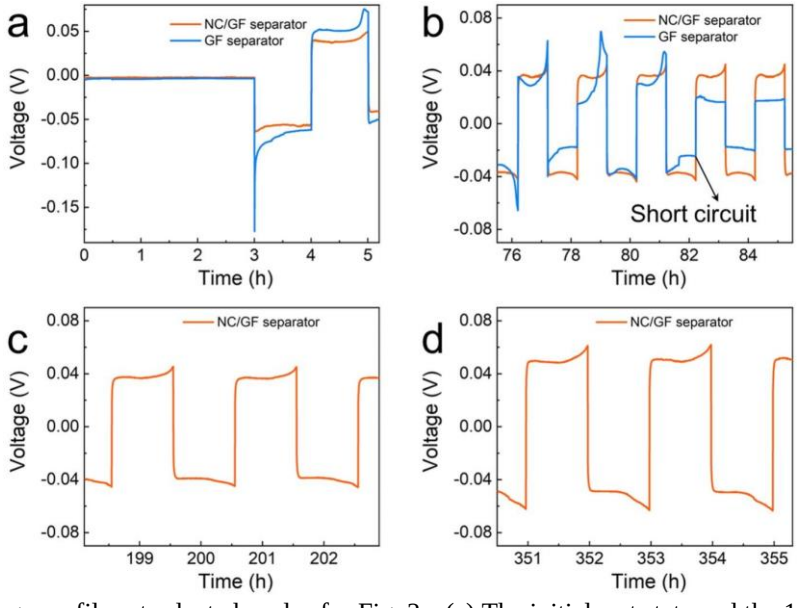

Figure S8 Enlarged voltage profiles at selected cycles for Fig. 2e. (a) The initial rest state and the 1st cycle. (b) The 36th-41st cycles. (c) The 98th-100th cycles. (d) The 174th-176th cycles.

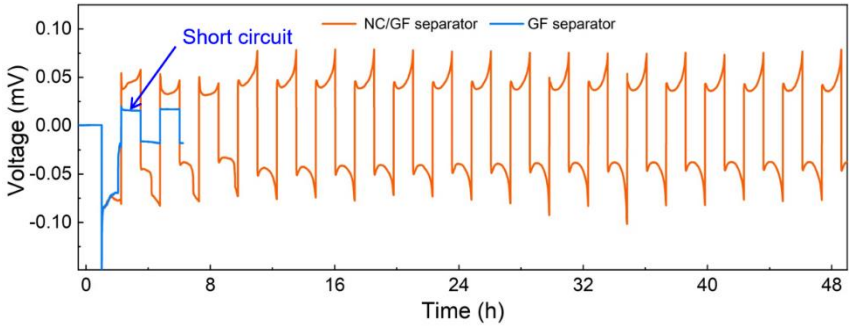

Figure S9 Galvanostatic cycling of Zn–Zn symmetric cells based on GF and NC/GF separator at a current density of 20 mA cm^{-2} and a capacity of 25 mAh cm^{-2}.

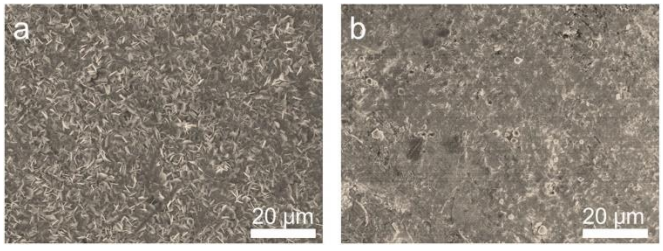

Figure S10 Top-view SEM images of Zn electrodes after 50 cycles at 1 mA cm^{-2}/1 mAh cm^{-2} assembled with (a) GF separator and (b) NC/GF separator.

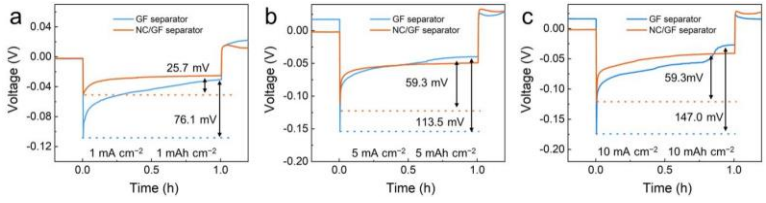

Figure S11 Nucleation overpotential for Zn–Zn symmetric cells with GF and NC/GF separator under different conditions: (a) 1 mA cm^{-2}/1 mAh cm^{-2}, (b) 5 mA cm^{-2}/5 mAh cm^{-2}, (c) 10 mA cm^{-2}/10 mAh cm^{-2}.

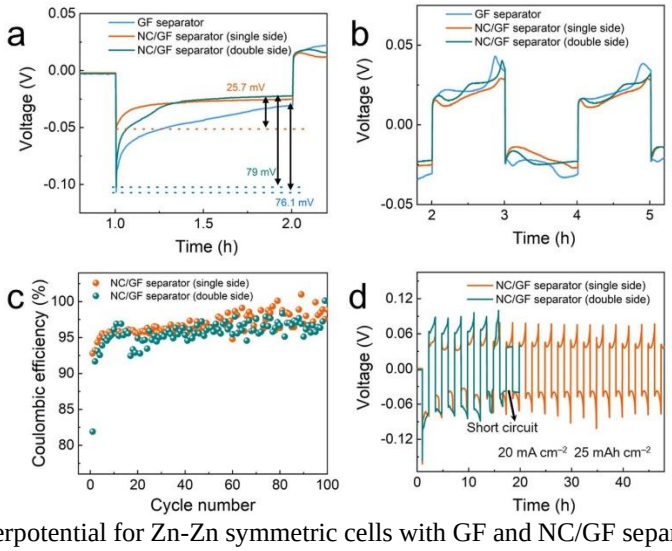

Figure S12. (a) Nucleation overpotential for Zn-Zn symmetric cells with GF and NC/GF separators under 1 mA cm^{-2}/1 mAh cm^{-2}. Here, NC/GF (single side) means that only one side of NC/GF separator was treated by air plasma. NC/GF (double side) denotes that both sides were treated by air plasma. (b) Voltage profiles at the initial plating/stripping stage. (c) CEs of Zn plating/stripping in Ti–Zn cells using NC/GF separators at a current density of 2 mA cm^{-2} and a capacity of 0.5 mAh cm^{-2}. (d) Galvanostatic cycling of Zn–Zn symmetric cells based on NC/GF separators at a current density of 20 mA cm^{-2} and a capacity of 25 mAh cm^{-2}.

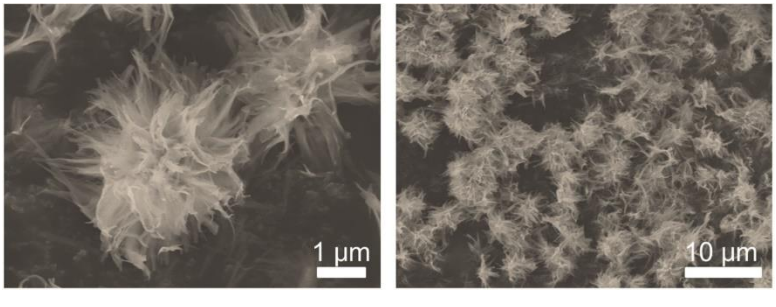

Figure S13 SEM images of KVOH nano-urchin architectures.

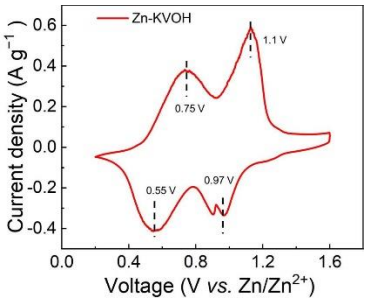

Figure S14 CV curve of a KVOH//Zn full cell equipped with NC/GF separator at a scan rate of 0.2 mV s^{-1}.

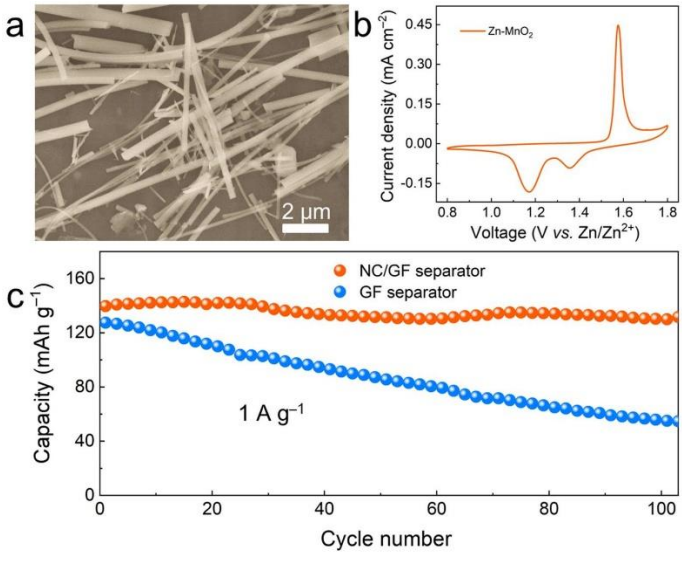

Figure S15 (a) SEM image of prepared MnO_2 nanorods. (b) CV curve of MnO_2//Zn full cell equipped with NC/GF separator at a scan rate of 0.2 mV s^{-1}. (c) Long-term cycling performance of MnO_2//Zn full cell equipped with NC/GF or bare GF separator at 1 A g^{-1}.

- **Supporting Table**

Table S1 Performance comparison of Zn anodes between this work and reported studies.

Materials	Areal current ($mA\ cm^{-2}$)	Areal capacity ($mAh\ cm^{-2}$)	Voltage hysteresis (mV)	Depth of discharge (DOD)	Lifespan	Ref.
***N*-doped carbon**	**1** **10** **20**	**1** **10** **25**	54 87 167	**42.7%**	1100 365 **48**	**This work**
Graphene oxide		2	100		500	[1]
Graphene	1 10	1 5	80 180	8.5%	250 80	[2]
Nitrogen-Doped Graphene	1 5	1 5	34 96	4.3%	1200 300	[3]
Nanoporous $CaCO_3$	0.25	0.05	104	0.2%	836	[4]
TiO_2 film	1	1	114		150	[5]
Nanoporous ZnO	5	1.25	84	2.1%	500	[6]
ZnO array	1	1	78		400	[7]
ZnS	2	2	70	17.1%	1100	[8]
$NaTi_2(PO_4)_3$	1	1	50		260	[9]
MXene	0.2 5	0.2 1	50 104	3.4%	800 100	[10]
Cyanoacrylate Adhesive	0.5 2	0.25 1	100 110	1.7%	800 400	[11]

Table S2 Parameters for calculating the ion transference number.

Separator	I_0 (μA)	I_s (μA)	R_0 (Ω)	R_s (Ω)	$T_{Zn^{2+}}$
GF	8.1	2.3	640	1909	0.26
NC/GF	44.3	23.6	219	412	0.57

Supporting References

[1] Cao, J.; Zhang, D.; Zhang, X.; Sawangphruk, M.; Qin, J.; Liu, R. A universal and facile approach to suppress dendrite formation for a Zn and Li metal anode. *J. Mater. Chem. A* **2020**, *8*, 9331-9344.

[2] Li, C.; Sun, Z.; Yang, T.; Yu, L.; Wei, N.; Tian, Z.; Cai, J.; Lv, J.; Shao, Y.; Rümmeli, M. H.; Sun, J.; Liu, Z. Directly grown vertical graphene carpets as Janus separators toward stabilized Zn metal anodes. *Adv. Mater.* **2020**, *32*, 2003425.

[3] Zhou, J.; Xie, M.; Wu, F.; Mei, Y.; Hao, Y.; Huang, R.; Wei, G.; Liu, A.; Li, L.; Chen, R. Ultrathin surface coating of nitrogen-doped graphene enables stable zinc anodes for aqueous zinc-ion batteries. *Adv. Mater.* **2021**, DOI: 10.1002/adma.202101649.

[4] Kang, L.; Cui, M.; Jiang, F.; Gao, Y.; Luo, H.; Liu, J.; Liang, W.; Zhi, C. Nanoporous $CaCO_3$ coatings enabled uniform Zn stripping/plating for long-life zinc rechargeable aqueous batteries. *Adv. Energy Mater.* **2018**, *8*, 1801090.

[5] Zhao, K.; Wang, C.; Yu, Y.; Yan, M.; Wei, Q.; He, P.; Dong, Y.; Zhang, Z.; Wang, X.; Mai, L. Ultrathin surface coating enables stabilized zinc metal anode. *Adv. Mater. Interfaces* **2018**, *5*, 1800848.

[6] Xie, X.; Liang, S.; Gao, J.; Guo, S.; Guo, J.; Wang, C.; Xu, G.; Wu, X.; Chen, G.; Zhou, J. Manipulating the ion-transfer kinetics and interface stability for high-performance zinc metal anodes. *Energy Environ. Sci.* **2020**, *13*, 503-510.

[7] Kim, J. Y.; Liu, G.; Shim, G. Y.; Kim, H.; Lee, J. K. Functionalized Zn@ZnO hexagonal pyramid array for dendrite-free and ultrastable zinc metal anodes. *Adv. Funct. Mater.* **2020**, *30*, 2004210.

[8] Hao, J.; Li, B.; Li, X.; Zeng, X.; Zhang, S.; Yang, F.; Liu, S.; Li, D.; Wu, C.; Guo, Z. An in-depth study of Zn metal surface chemistry for advanced aqueous Zn-ion batteries. *Adv. Mater.* **2020**, *32*, 2003021.

[9] Liu, M.; Cai, J.; Ao, H.; Hou, Z.; Zhu, Y.; Qian, Y. $NaTi_2(PO_4)_3$ solid-state electrolyte protection layer on Zn metal anode for superior long-life aqueous zinc-ion batteries. *Adv. Funct. Mater.* **2020**, *30*, 2004885.

[10] Zhang, N.; Huang, S.; Yuan, Z.; Zhu, J.; Zhao, Z.; Niu, Z. Direct self-assembly of MXene on Zn anodes for dendrite-free aqueous zinc-ion batteries. *Angew. Chem. Int. Ed.* **2020**, *60*, 2861-2865.

[11] Cao, Z.; Zhu, X.; Xu, D.; Dong, P.; Chee, M. O. L.; Li, X.; Zhu, K.; Ye, M.; Shen, J. Eliminating Zn dendrites by commercial cyanoacrylate adhesive for zinc ion battery. *Energy Storage Mater.* **2021**, *36*, 132-138.